# Improving Gyroscope's Noise Performance Using Multiple Accelerometers in a Closed-Loop Configuration

Konstantinos Papafotis, *Member, IEEE*, Dimitris Nikitas, and Paul P. Sotiriadis, *Senior Member, IEEE*

***Abstract*—An inertial measurement unit (IMU) architecture is proposed by combining a set of accelerometers with a three-axis gyroscope, in closed-loop operation, to achieve superior accuracy and low noise estimation of the angular velocity by compensating for accelerometers' bias and wandering. It advances the concept of gyroscope-free IMUs, which derive the angular velocity using multiple accelerometers in an open-loop configuration, by eliminating their constant drift errors due to accelerometers' bias, enabling real-world applications. The stability of the proposed closed-loop system is studied analytically with sufficient conditions provided, and a closed-form expression of the angular velocity noise is derived. Both experimental and simulation results indicate that the proposed architecture excels in terms of accuracy and noise performance.**

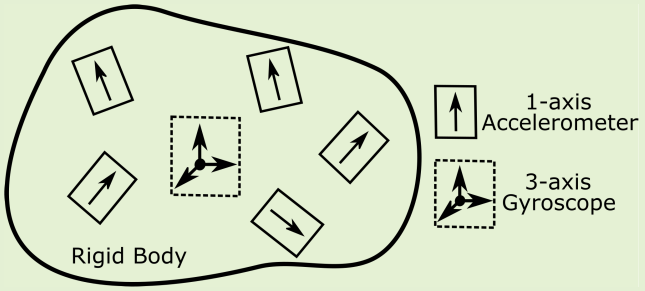


***Index Terms*—Accelerometer, closed-loop, gyroscope, inertial measurement unit (IMU), low-noise.**

## I. Introduction

INERTIAL sensors (accelerometers and gyroscopes) are nowadays embedded in several commercial devices such as smartphones, activity trackers, alarm systems, and others, while they are also used in many high-end, industrial, marine, aerospace, and military applications. The fast development of micro-electro-mechanical (MEM) inertial sensors over the past decades enabled the wider use of inertial sensors. Their miniature size and extremely low cost make MEM inertial sensors the ideal choice for a plethora of applications. However, their large error characteristics and measurement noise [1] forbid their use in applications where measurement accuracy is important.

The measurement errors sourcing from manufacturing imperfections are (in their greatest part) static and there are several calibration techniques that can effectively compensate for them [2], [3], [4], [5], [6], [7].

The nondeterministic measurement noise, on the other hand, is a more complicated problem that is most commonly dealt with using extra sensors or estimation and filtering techniques according to the specific application's specifications and needs. In inertial navigation, for example, where the gyroscope's noise is causing a significant attitude error [8], it is common to use a Kalman filter [1], [9], [10] or use additional sensors, such as a magnetometer [1], [11], [12], to get a more accurate attitude estimation.

A class of inertial measurement units (IMUs), known as gyroscope-free IMUs (GF-IMUs), use several accelerometers mounted on a rigid object to provide an estimation of both the specific force and the angular velocity of the object. When the accelerometers are spread over a wide distance, GF-IMUs provide a very low-noise estimation of the angular velocity compared to a gyroscope of the same grade.

However, GF-IMUs come with a big disadvantage, making them inappropriate for real-world applications. More specifically, GF-IMUs cannot compensate for the accelerometers' bias; even a small bias on the accelerometers' output is translated into a constant drift in the estimated angular velocity.

This work introduces an IMU architecture that combines several single-axis accelerometers and a single three-axis gyroscope, in a closed-loop configuration. The proposed architecture extends the existing GF-IMU architectures and compensates for the effects of the accelerometers' bias while it provides a very low-noise angular velocity estimation. The introduced system is theoretically analyzed and its stability is

Manuscript received 16 July 2022; revised 30 August 2022; accepted 31 August 2022. Date of publication 21 September 2022; date of current version 14 November 2022. This work was supported in part by the Greece and the European Union [European Social Fund (ESF)] through the Operational Program "Human Resources Development, Education and Lifelong Learning" in the Context of the Project "Strengthening Human Resources Research Potential via Doctorate Research" Implemented by the State Scholarships Foundation (IKY) under Grant MIS-5000432, and in part by the European Union-NextGenerationEU and Greek National Funds through the Greece 2.0 National Recovery and Resilience Plan, under the call RESEARCH-CREATE-INNOVATE PROJECT CODE TAEDK-06165. The associate editor coordinating the review of this article and approving it for publication was Prof. Chang-Hee Won. *(Corresponding author: Konstantinos Papafotis.)*

The authors are with the Department of Electrical and Computer Engineering, National Technical University of Athens, 15780 Athens, Greece (e-mail: k.papafotis@gmail.com).

Digital Object Identifier 10.1109/JSEN.2022.3207110

proven analytically. In addition, a closed-form expression for the output angular velocity noise is derived. Both experimental and simulation results indicate that the proposed system excels in terms of noise performance; in the upper frequency range, it can provide up to 30 dB less noise at its output compared to the gyroscope.

The rest of this work is structured as follows. In Section II, the basic operation principles of the gyroscope-free inertial measurement systems are introduced and two popular architectures are presented while their main performance limitations are highlighted. In Section III, the proposed closed-loop architecture is introduced and analyzed in detail. Its stability is analytically proved, and a closed-form expression for its output noise is derived. In Section IV, extensive simulations as well as experimental measurements are presented to evaluate the performance of the proposed system. Finally, conclusions are drawn in Section V.

## II. Gyroscope-Free Inertial Measurement Systems

In this section, the basic principle of GF-IMUs is introduced. Then, two popular and highly cited architectures are presented to highlight the performance limitations of the class of GF-IMUs.

### A. Principle of Operation

Consider $N$ single-axis accelerometers, placed at arbitrary positions, $r_i, i = 1, 2, \ldots, N$ on a rigid body and denote their sensitivity axes and measurements as $\hat{\eta}_i$ and $f_i$, respectively. Following [13], we write the following system of equations for deriving the specific force ($f$) and the angular velocity ($\omega$):

$$F = Jx + P \tag{1}$$

where

$$x = \begin{bmatrix} \dot{\omega} \\ f \end{bmatrix}, \quad J = \begin{bmatrix} J_1^T & J_2^T \end{bmatrix}$$
$$F = \begin{bmatrix} f_1 \\ f_2 \\ \vdots \\ f_N \end{bmatrix}, \quad P = \begin{bmatrix} \hat{\eta_1}^T \Omega^2 r_1 \\ \hat{\eta_2}^T \Omega^2 r_2 \\ \vdots \\ \hat{\eta_N}^T \Omega^2 r_N \end{bmatrix} \tag{2}$$

the auxiliary variables $J_1$ and $J_2$ are

$$J_1 = \begin{bmatrix} (r_1 \times \hat{\eta}_1) & (r_2 \times \hat{\eta}_2) & \cdots & (r_N \times \hat{\eta_N}) \end{bmatrix}$$
$$J_2 = \begin{bmatrix} \hat{\eta}_1 & \hat{\eta}_2 & \cdots & \hat{\eta_N} \end{bmatrix} \tag{3}$$

and $\Omega$ is the cross-product matrix of the vector $\omega \triangleq \begin{bmatrix} \omega_x & \omega_y & \omega_z \end{bmatrix}^T$

$$\Omega = \begin{bmatrix} 0 & -\omega_z & \omega_y \\ \omega_z & 0 & -\omega_x \\ -\omega_y & \omega_x & 0 \end{bmatrix}. \tag{4}$$

Given an adequate number of properly placed (single-axis) accelerometers, one can solve (1) in a least-squares sense and derive $x$ as

$$x = \left(J^T J\right)^{-1} J^T (F - P). \tag{5}$$

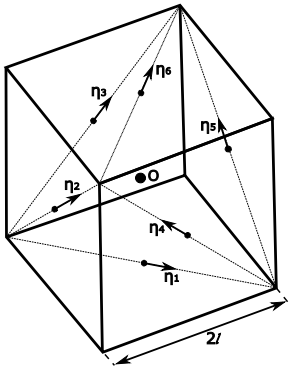


Fig. 1. Gyroscope-free inertial measurement system proposed in [13]. Six single-axis accelerometers are placed on the faces of a cube. Their sensitivity axes are denoted by $\hat{\eta_1}, \hat{\eta_2}, \ldots, \hat{\eta_6}$.

Further defining $\bar{J} = (J^T J)^{-1} J^T$, (5) is written in a compact form as

$$x = \bar{J}F - \bar{J}P \tag{6}$$

and the solution is only valid if $J^T J$ is nonsingular.

In this work, we focus on the solution of the system of differential equations for deriving the angular velocity $\omega$. Denoting the $i$th row of $\bar{J}$ as $\bar{J}_i$, we write

$$\dot{\omega} = \hat{J}F - \hat{J}P \tag{7}$$

where

$$\hat{J} = \begin{bmatrix} \bar{J}_1^T & \bar{J}_2^T & \bar{J}_3^T \end{bmatrix}^T. \tag{8}$$

### B. Existing Art and Performance Limitations

Several GF-IMU architectures have been proposed over the years. Many authors have proposed architectures using six [13], nine [14], [15], [16], ten [17], or 12 [18], [19] (single-axis) accelerometers in an effort to provide a feasible solution to (7) and moreover simplify the original nonlinear problem for estimating the angular velocity.

To demonstrate the performance limitations of the existing systems using multiple accelerometers in open-loop configuration, we consider two popular ones: the cube-type IMU proposed by Chen *et al.* [13] and further studied by several other authors [20], [21], [22], [23], [24], [25] and the nine accelerometers system proposed in [16].

Chen *et al.* [13] use just six single-axis accelerometers placed on the faces of a cube as shown in Fig. 1. By doing so, the nonlinear terms of (7) are eliminated and the derivative of the angular velocity is derived as a linear combination of the six accelerometers' measurements as follows:

$$\dot{\omega}_6 = \frac{1}{2l^2} J_6 F_6 \tag{9}$$

where

$$J_6 \triangleq \begin{bmatrix} (r_1 \times \hat{\eta}_1) & (r_2 \times \hat{\eta}_2) & \cdots & (r_6 \times \hat{\eta}_6) \end{bmatrix} \tag{10}$$

and $F_6$ is the $6 \times 1$ vector of the accelerometers' measurements.

Similarly, a combination of nine properly placed accelerometers is proposed in [16]. The proposed configuration, shown in

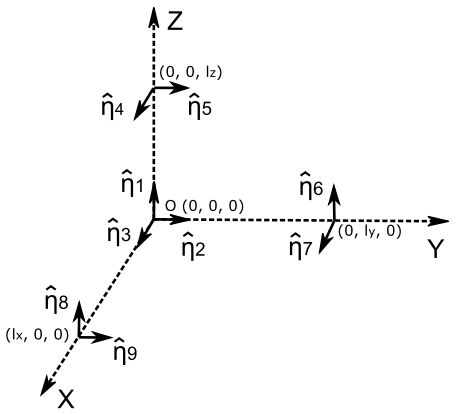


Fig. 2. Gyroscope-free inertial measurement system proposed in [16]. Nine single-axis accelerometers are placed on a rigid body. Their sensitivity axes are denoted by $\hat{\eta_1}, \hat{\eta_2}, \ldots, \hat{\eta_9}$.

Fig. 2, also results in a linear system of differential equations for calculating the angular velocity

$$\dot{\omega_9} = J_9 F_9 \tag{11}$$

where $J_9$ is defined according to (12) as shown at the bottom of the next page, and $F_9$ is the $9 \times 1$ vector of the accelerometers' measurements.

Inspecting (9) and (11), one realizes that they share the same form; in both cases, the derivative of the angular velocity is equal to a linear combination of the accelerometers' measurements. A further investigation of the relevant literature reveals that this is the case in all similar works on GF-IMUs [13], [14], [15], [16], [17], [18], [19]. Thus, we write a general expression for the output angular velocity of an GF-IMU consisting of $N$ accelerometers

$$\dot{\omega_N} = J_N F_N \tag{13}$$

where $J_N$ a $3 \times N$ matrix and $F_N$ is the $N \times 1$ vector of the accelerometers' measurements.

While the aforementioned works provide a very simple and computationally light solution to the original nonlinear problem, the analysis is limited to the case of ideal accelerometers and neglects the effects of noise, bias, and other imperfections of a real-world accelerometer. Since the bias is the largest contributor to the accelerometer's measurement error [2], we will examine the effect of a small additive bias, $\delta F_N$ on the accelerometer's measurements. In this case, (13) becomes

$$\dot{\tilde{\omega}_N} = J_N(F_N + \delta F_N) \tag{14}$$

where $\delta F_N$ is the $N \times 1$ vectors representing the accelerometers' bias. Subtracting (13) from (14), we get the evolution of the system's output error in time

$$\delta\dot{\omega}_N \triangleq \dot{\omega_N} - \dot{\tilde{\omega}_N} = J_N \delta F_N. \tag{15}$$

As seen in (15), the output error of the existing systems accumulates over time meaning that even a very small offset in the accelerometers' measurements causes a cumulative angular velocity error. This is rather important as even if the static sensors' offset is removed by a calibration procedure, a small offset drift is expected over time, especially in the case of low-cost sensors.

## III. Proposed System

In this section, the proposed inertial measurement system is introduced and analyzed in detail. The stability of the proposed system under the effects of the accelerometers' and gyroscope's biases is investigated. Finally, the system's output angular velocity noise is analytically derived in closed form.

### A. System Analysis

To alleviate the performance limitations of existing architectures, presented in Section II-B, the proposed system uses a three-axis gyroscope, placed at the origin of the body frame (point O in Figs. 1 and 2). The top-level architecture of the proposed system is shown in Fig. 3(a) and its block diagram representation is shown in Fig. 3(b).

In open-loop operation, the accelerometers' measurements ($F$) pass through a linear system according to (13) to result into the angular acceleration ($\dot{\omega}$). Then, the angular acceleration is integrated to derive the angular velocity ($\omega$). The feedback loop uses the gyroscope's measurements to derive an estimation of the error between the open-loop system's output and the actual value of the angular velocity. This error estimation is fed back through a low-pass filter to compensate for the accelerometers' bias and measurement errors.

Intuitively, the feedback loop that is introduced forces the output of the system to be equal to one of the gyroscopes at lower frequencies, before the low-pass filter's cutoff frequency. At higher frequencies, the feedback signal is attenuated and the system's output is dominated by the accelerometers' measurements.

As illustrated in Fig. 3, the proposed system is a multiple-input, single-output (MISO) one and thus the standard performance metrics of the classical control theory (e.g., bandwidth, phase margin, gain margin) cannot be used [26]. However, as far as the frequency response of the proposed system is concerned, the cut-off frequency of the low-pass filter of the feedback loop is typically set to a low frequency, up to a couple of Hz, much lower than the bandwidth of a typical accelerometer or gyroscope. In the higher frequency band, the feedback signal is attenuated significantly and the system practically operates in an open loop. Thus, the proposed closed-loop system comes with no bandwidth tradeoff.

Before continuing with the analysis of the system and since both the inputs ($F$ and $\omega_g$) and the output ($\omega$) of the system are

$$J_9 \triangleq \begin{bmatrix} -\frac{1}{2l_y} & \frac{1}{2l_z} & 0 & 0 & -\frac{1}{2l_z} & \frac{1}{2l_y} & 0 & 0 & 0 \\ \frac{1}{2l_x} & 0 & -\frac{1}{2l_z} & \frac{1}{2l_z} & 0 & 0 & 0 & -\frac{1}{2l_x} & 0 \\ 0 & -\frac{1}{2l_x} & \frac{1}{2l_y} & 0 & 0 & 0 & -\frac{1}{2l_y} & 0 & \frac{1}{2l_x} \end{bmatrix} \tag{12}$$

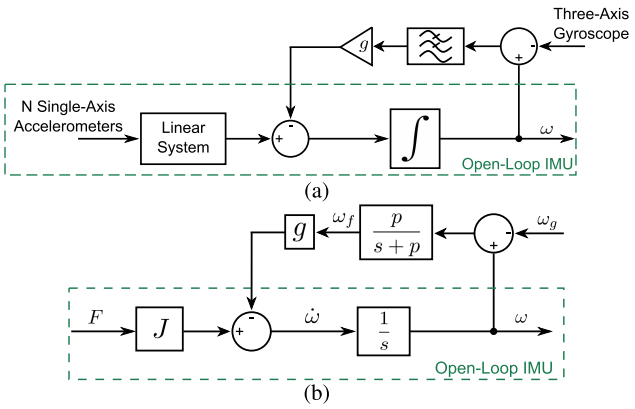


Fig. 3. (a) Top-level architecture and (b) block diagram representation of the proposed system.

vectors, it is useful to define the following diagonal matrices related to the modeling of the feedback loop:

$$\begin{aligned} G &= I_3 \otimes g \\ P &= I_3 \otimes p \\ P_s &= I_3 \otimes \left(\frac{p}{s+p}\right) \end{aligned} \tag{16}$$

where $I_3$ is the $3 \times 3$ identity matrix and $\otimes$ denotes the Kronecker's product [27]. Assume that the input measurements of both the accelerometer [$F$ in Fig. 3(b)] and the gyroscope [$\omega_g$ in Fig. 3(b)] are not ideal and it is

$$F = F_i + \delta F \quad \text{and} \quad \omega_g = \omega_{gi} + \delta\omega_g \tag{17}$$

where $F_i \in \mathbb{R}^6$ and $\omega_{gi} \in \mathbb{R}^3 \triangleq \omega$ are the ideal measurements of the accelerometers and the gyroscope, respectively, and $\delta F \in \mathbb{R}^6$ and $\delta\omega_g \in \mathbb{R}^3$ represent the measurement error of the two sensors. Using this assumption and following the block diagram of Fig. 3(b), we write:

$$\dot{\tilde{\omega}} = J(F_i + \delta F) - G\omega_f. \tag{18}$$

Using (18) and the ideal output of the open-loop system derived in (13), we get the evolution of the system's output error in time

$$\dot{\delta\omega} = J\delta F - G\omega_f. \tag{19}$$

Following Fig. 3(b), the feedback signal is written as:

$$\begin{aligned} \omega_f &= P_s(\tilde{\omega} - \omega_{gi} - \delta\omega_g) \\ &= P_s(\delta\omega - \delta\omega_g) \end{aligned} \tag{20}$$

and its time derivative is derived as

$$\dot{\omega_f} = -P\ \omega_f + P(\delta\omega - \delta\omega_g). \tag{21}$$

Using (19) and (21), we write the following state-space system representation:

$$\underbrace{\begin{bmatrix} \dot{\delta\omega} \\ \dot{\omega_f} \end{bmatrix}}_{\dot{x}} = \underbrace{\begin{bmatrix} 0_{3\times3} & -G \\ P & -P \end{bmatrix}}_{A} \underbrace{\begin{bmatrix} \delta\omega \\ \omega_f \end{bmatrix}}_{x} + \underbrace{\begin{bmatrix} J & 0_{3\times3} \\ 0_{3\times6} & -P \end{bmatrix}}_{B} \underbrace{\begin{bmatrix} \delta F \\ \delta\omega_g \end{bmatrix}}_{u}. \tag{22}$$

The characteristic polynomial of $A$ is

$$p_A(\lambda) = (\lambda^2 + p\lambda + gp)^3 \tag{23}$$

and its roots (which are the eigenvalues of $A$) are always negative for positive values of $g$ and $p$. Thus, $A$ is always Hurwitz and the system of (22) is bounded-input bounded-output (BIBO) stable. This is an important result as it indicates that the output error of the proposed system, $\delta\omega$, is bounded for bounded inputs of the accelerometers' and the gyroscope's biases, $\delta F$ and $\delta\omega_g$, respectively.

To quantify the effect of the accelerometers' and the gyroscope's biases on the system's output error, we assume a small constant bias vector $\bar{f} \in \mathbb{R}^6$ for the accelerometers and a small constant bias vector $\bar{\omega} \in \mathbb{R}^3$ for the gyroscope. From (22), we get

$$\begin{aligned} x(t) &= e^{At}x(0) + \int_0^t e^{A(t-s)}B\begin{bmatrix}\bar{f}\\ \bar{\omega}\end{bmatrix}\mathrm{ds} \\ &= e^{At}x(0) + (e^{At} - I_6)A^{-1}B\begin{bmatrix}\bar{f}\\ \bar{\omega}\end{bmatrix} \end{aligned} \tag{24}$$

where $I_6$ is the $6 \times 6$ identity matrix. The steady-state response of (22) is derived as

$$\begin{aligned} \lim_{t\to+\infty} x(t) &= -A^{-1}B\begin{bmatrix}\bar{f}\\ \bar{\omega}\end{bmatrix} \\ &= \begin{bmatrix} \dfrac{J\bar{f}}{g} + \bar{\omega} \\ \dfrac{\bar{f}}{g} \end{bmatrix} \end{aligned} \tag{25}$$

and consequently

$$\delta\omega\big|_{t\to+\infty} = \frac{J\bar{f}}{g} + \bar{\omega}. \tag{26}$$

The result of (26) is quite interesting as it indicates that in the steady state, the proposed system's offset is composed of a small portion of the accelerometers' bias and the whole gyroscope's bias. This comes in agreement with our intuition about the system's operation; the feedback loop forces the system's output to be equal to the gyroscope's one in low frequencies. Using the triangle inequality and (25), we get the worst-case scenario for the steady-state value of $\delta\omega$ which is

$$\|\delta\omega\| \le \left\|\frac{J\bar{f}}{g}\right\| + \|\bar{\omega}\| \tag{27}$$

and represents the case when the effect of the accelerometers' and the gyroscope's bias is additive.

### B. Output Noise Modeling

We consider the proposed system's block diagram representation of Fig. 3(b). Since the system is linear, we use superposition to calculate the output angular velocity as a function of the two inputs: the accelerometers' measurements ($F$) and the gyroscope's measurement ($\omega_g$). More specifically, it is

$$\omega(s) = (I_3 \otimes H_F(s))\,\hat{F}(s) + \left(I_3 \otimes H_g(s)\right)\omega_g(s) \tag{28}$$

where

$$\begin{aligned} H_F(s) &= \frac{s+p}{s^2+ps+gp} \\ H_g(s) &= \frac{gp}{s^2+ps+gp} \end{aligned} \tag{29}$$

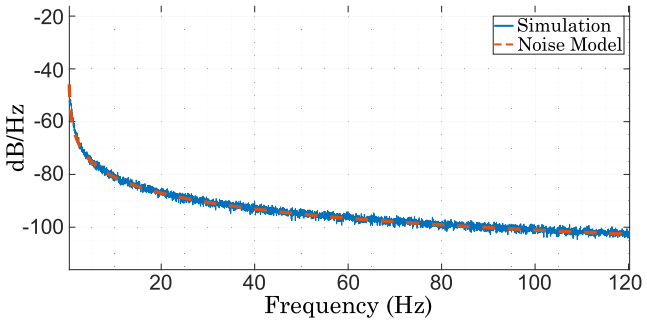


Fig. 4. PSD of the output of the proposed system compared to the PSD calculated using the noise model of (31).

and

$$\hat{F}(s) = JF(s). \tag{30}$$

Denote the power spectral density (PSD) of the gyroscope's measurement as $S_g(s)$ and the PSD of $\hat{F}$ as $S_{\hat{F}}(s)$. Assuming that the output noise of the accelerometers and the gyroscope are uncorrelated, the PSD of the output angular velocity, $S_\omega$, is derived as follows:

$$S_\omega(s) = \left(I_3 \otimes |H_F(s)|^2\right) S_{\hat{F}}(s) + \left(I_3 \otimes |H_g(s)|^2\right) S_g(s) \tag{31}$$

where

$$|H_F(s)|^2 = \frac{-s^2 + p^2}{s^4 + (2gp - p^2)s^2 + g^2p^2}$$
$$|H_g(s)|^2 = \frac{g^2p^2}{s^4 + (2gp - p^2)s^2 + g^2p^2}. \tag{32}$$

The exact characteristics of the accelerometers' and the gyroscope's noise depend on the sensor used and are different even along sensors using the same manufacturing technology. However, typically, the noise of the accelerometers and the gyroscope is considered to be white noise. This is a reasonable assumption used in many works to facilitate mathematical analysis and in most cases gives accurate results.

We assume that both the inputs $F$ and $\omega_g$ are excited with white noise, that is,

$$F \sim \mathcal{N}(0, C_F) \quad \text{and} \quad \omega_g \sim \mathcal{N}(0, C_\omega) \tag{33}$$

where $C_F$ and $C_\omega$ denote the covariance of the accelerometers' and gyroscope's noise, respectively. The noise of the linear combination of the accelerometers' measurements, $JF$, is also white noise with covariance $C_{JF} = JC_FJ^T$ [28] and thus it is

$$\hat{F} \sim \mathcal{N}(0, C_{JF}). \tag{34}$$

In this case, the PSD of the output angular velocity, $S_\omega$, is derived as follows:

$$S_\omega(s) = \left(I_3 \otimes |H_F(s)|^2\right)(J \circ J)S_F + \left(I_3 \otimes |H_g(s)|^2\right) S_g \tag{35}$$

where $S_F$ is the PSD of the accelerometers' noise.

The accuracy of the derived noise model was verified via simulations in MATLAB's Simulink. More specifically, both inputs of the proposed system ($F$ and $\omega_g$) were excited with a random white noise; the PSD of the output angular velocity is shown in Fig. 4 along with the PSD calculated using (31).

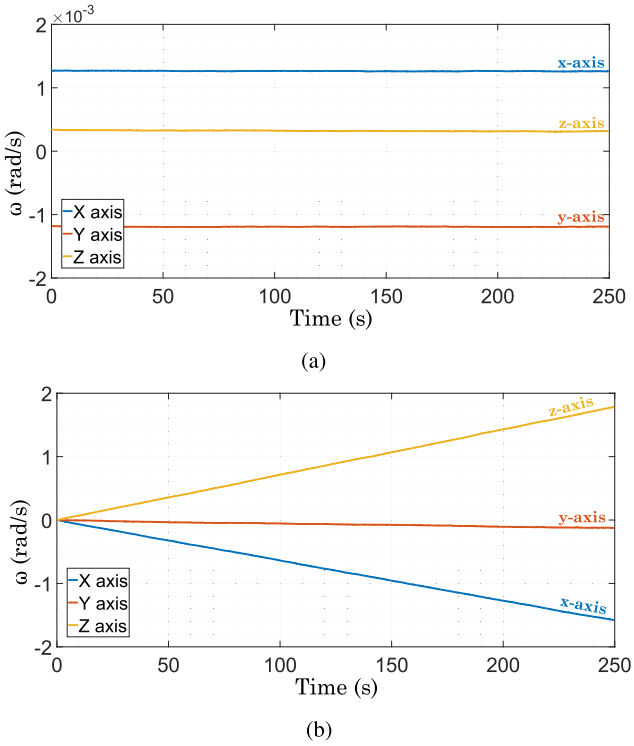


Fig. 5. (a) Output angular velocity of the proposed system. (b) Compared to the output angular velocity of [13]. Both systems are excited with a small, constant offset and white noise.

## IV. Performance Evaluation

To evaluate the performance of the proposed system, we performed a series of simulations using MATLAB's Simulink. In addition, we used low-cost inertial sensors to capture experimental measurements from a real-world implementation of the IMU architecture of Fig. 2 and confirm the performance characteristics of the proposed system in real-world conditions.

### A. Simulation Results

The effect of sensors' bias and noise is examined by exciting all the accelerometers and the gyroscope with a small, constant bias and white noise. In Fig. 5, the output of the proposed system using the cube configuration of Fig. 1 is compared to the one of the open-loop system introduced in [13]. As seen in Fig. 5(a), the proposed system outputs a small constant over time bias on the contrary to the open-loop system [Fig. 5(b)], the output of which drifts significantly over time.

Next, the noise performance of the proposed system is evaluated. To do so, we used the cube configuration of Fig. 1 and excited both the accelerometers' and the gyroscope's inputs of the system of Fig. 3(b) with band-limited white noise. The noise characteristics were chosen to match the ones of a popular IMU in chip form [29]. The feedback's gain was set to $g = 20$ while the cut-off frequency of the low-pass filter was set to $p = 2\pi 0.5$ rad (0.5 Hz).

The PSD of the system's output is presented in Fig. 6 and compared to the PSD of the gyroscope's noise for two different values of the parameter $l$ in Fig. 1 which determines the distance between the accelerometers. As seen in Fig. 6, while the distance between the accelerometers gets longer, the output noise of the proposed system gets significantly lower in the higher frequencies (up to 30 dB lower than the

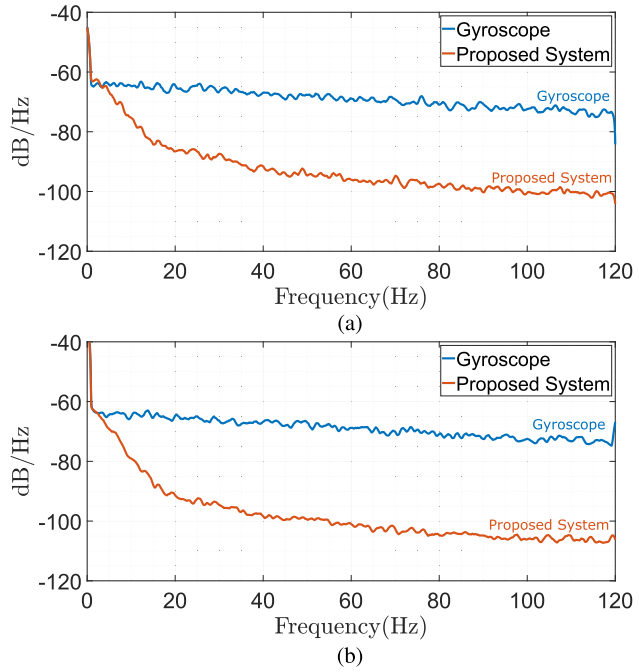


Fig. 6. PSD of the proposed system's output noise (*X*-axis) compared to the PSD of the gyroscope's output noise (*X*-axis) for (a) $l = 0.5$ m and (b) $l = 2$ m.

TABLE I
PERFORMANCE CHARACTERISTICS OF THE ACCELEROMETER (A) AND THE GYROSCOPE (G) INCLUDED IN THE LSM9DS1 SIP

| Specification | Value |
|---|---|
| Measurement Range (A) | $\pm 16g$ |
| Measurement Range (G) | $\pm 2000dps$ |
| Sampling Rate (A) | $238Hz$ |
| Sampling Rate (G) | $238Hz$ |
| Resolution (A, G) | $16Bits$ |

one of the gyroscope) where the output is dominated by the accelerometers' measurements.

### B. Experimental Results

To evaluate the performance of the proposed system in real-world conditions, we used the IMU architecture of Fig. 2. The experimental setup, shown in Fig. 7, is composed of a laser-cut steel frame and four modules embedding the low-cost LSM9DS1 system-in-package (SiP) by STMicroelectronics to capture the specific force and the angular velocity measurements. While every LSM9DS1 module includes a three-axis accelerometer and a three-axis gyroscope, for our experiments we only used the acceleration measurements in the directions $\hat{\eta}_1 - \hat{\eta}_9$ denoted in Fig. 7 and three-axis gyroscope measurements from the module placed at the origin (O). The sensors were sampled at a rate of 238 Hz by a 32-bit microcontroller (STM32F746) and the measurements were sent to a computer for processing. The sensors' distance is set to $l_x = l_y = l_z = 0.5$ m according to Fig. 2.

Some important performance characteristics of the accelerometer and the gyroscope included in the LSM9DS1 SiP are presented in Table I.

Using the experimental setup of Fig. 7, we measured the PSD of the angular velocity noise using the proposed system and compared it to the PSD of the gyroscope's noise. As indicated in Fig. 8, the experimental results come in agreement with both the theoretical analysis and the MATLAB simulations. In the upper frequency range, the output noise of the proposed system is up to 25 dB lower compared to the one of the gyroscope.

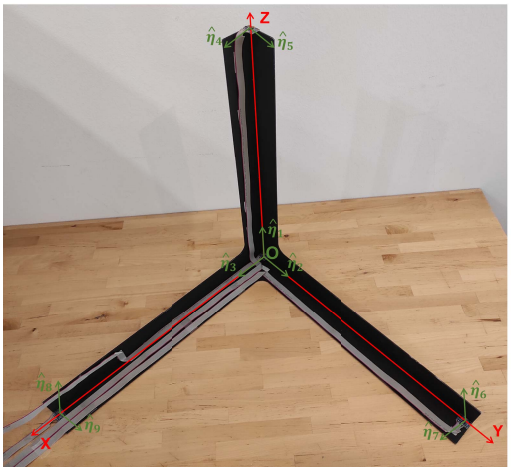


Fig. 7. Experimental setup of the nine-accelerometer architecture of Fig. 2 with $l_x = l_y = l_z = 0.5$ m.

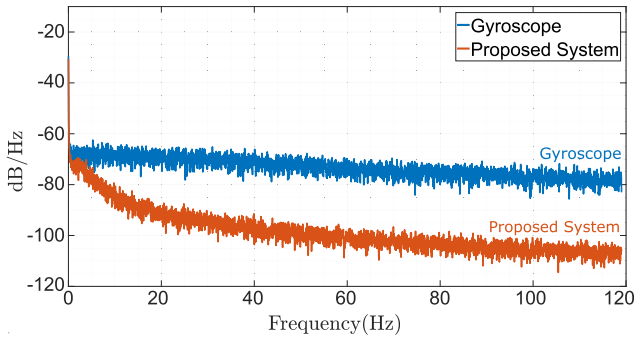


Fig. 8. PSD of the proposed system's output noise (*X*-axis) compared to the PSD of the gyroscope's output noise using the experimental setup of Fig. 7.

## V. CONCLUSION

In this work, we introduced a new IMU architecture that expands a big class of existing systems and makes them robust for use in real-world conditions. We demonstrated how existing works cannot be used with real sensors' data as they cannot compensate for the accelerometers' bias. Then, we analytically proved the ability of the proposed system to compensate for the accelerometers' bias. Furthermore, we compared the output noise of the proposed system to the one of a gyroscope of the same grade. We demonstrated that when the accelerometers are spread over a great distance, the output noise of the proposed system is up to 30 dB lower than the one of the gyroscope.

## REFERENCES

[1] P. D. Groves, *Principles of GNSS, Inertial, and Multisensor Integrated Navigation Systems*. Norwood, MA, USA: Artech House, 2013.
[2] K. Papafotis and P. P. Sotiriadis, "MAG.I.C.AL.—A unified methodology for magnetic and inertial sensors calibration and alignment," *IEEE Sensors J.*, vol. 19, no. 18, pp. 8241–8251, Sep. 2019.
[3] K. Papafotis and P. P. Sotiriadis, "Multiple accelerometers and magnetometers joint calibration and alignment," *IEEE Sensors Lett.*, vol. 4, no. 3, pp. 1–4, Feb. 2020.

[4] M. Kok, J. D. Hol, T. B. Schön, F. Gustafsson, and H. Luinge, "Calibration of a magnetometer in combination with inertial sensors," in *Proc. 15th Int. Conf. Inf. Fusion*, Jul. 2012, pp. 787–793.
[5] J. F. Vasconcelos *et al.*, "Geometric approach to strapdown magnetometer calibration in sensor frame," *IEEE Trans. Aerosp. Electron. Syst.*, vol. 47, no. 2, pp. 1293–1306, Apr. 2011.
[6] Y. Wu and W. Shi, "On calibration of three-axis magnetometer," *IEEE Sensors J.*, vol. 15, no. 11, pp. 6424–6431, Nov. 2015.
[7] E. Dorveaux, D. Vissière, A.-P. Martin, and N. Petit, "Iterative calibration method for inertial and magnetic sensors," in *Proc. 48th IEEE Conf. Decis. Control (CDC)*, Dec. 2009, pp. 8296–8303.
[8] K. Papafotis and P. P. Sotiriadis, "Exploring the importance of sensors' calibration in inertial navigation systems," in *Proc. IEEE Int. Symp. Circuits Syst. (ISCAS)*, Oct. 2020, pp. 1–4.
[9] A. Noureldin, T. B. Karamat, and J. Georgy, *Fundamentals of Inertial Navigation, Satellite-based Positioning and Their Integration*. Berlin, Germany: Springer-Verlag, 2013.
[10] R. Stirling, J. Collin, K. Fyfe, and G. Lachapelle, "An innovative shoe-mounted pedestrian navigation system," in *Proc. Eur. Navigat. Conf. GNSS*, 2003, pp. 5–110.
[11] P. Groves, G. Pulford, C. Littlefield, D. Nash, and C. Mather, "Inertial navigation versus pedestrian dead reckoning: Optimizing the integration," in *Proc. 20th Int. Tech. Meeting Satell. Division Inst. Navigat.*, vol. 2, 2007, pp. 2043–2055.
[12] J. Bird and D. Arden, "Indoor navigation with foot-mounted strapdown inertial navigation and magnetic sensors [emerging opportunities for localization and tracking]," *IEEE Wireless Commun.*, vol. 18, no. 2, pp. 28–35, Apr. 2011.
[13] J.-H. Chen, S.-C. Lee, and D. B. DeBra, "Gyroscope free strapdown inertial measurement unit by six linear accelerometers," *J. Guid., Control, Dyn.*, vol. 17, no. 2, pp. 286–290, 1994, doi: 10.2514/3.21195.
[14] F. Qin, J. Xu, and J. Sai, "A new scheme of gyroscope free inertial navigation system using 9 accelerometers," in *Proc. Int. Workshop Intell. Syst. Appl.*, May 2009, pp. 1–4.
[15] J. Genin, J. Hong, and W. Xu, "Accelerometer placement for angular velocity determination," *J. Dyn. Syst., Meas., Control*, vol. 119, no. 3, pp. 474–477, Sep. 1997, doi: 10.1115/1.2801281.
[16] A. J. Padgaonkar, K. W. Krieger, and A. I. King, "Measurement of angular acceleration of a rigid body using linear accelerometers," *J. Appl. Mech.*, vol. 42, no. 3, pp. 552–556, Sep. 1975, doi: 10.1115/1.3423640.
[17] A. Li, F. J. Qin, and J. N. Xu, "Gyroscope free strapdown inertial navigation system using rotation modulation," in *Proc. 2nd Int. Conf. Intell. Comput. Technol. Automat.*, vol. 3, 2009, pp. 611–614.
[18] F.-J. Qin, J.-N. Xu, and A. Li, "A novel attitude algorithm for 12 accelerometer based GFINS using Hermite interpolation," in *Proc. Int. Conf. Measuring Technol. Mechatronics Autom.*, vol. 1, 2010, pp. 214–217.
[19] E. Edwan, S. Knedlik, and O. Loffeld, "Constrained angular motion estimation in a gyro-free IMU," *IEEE Trans. Aerosp. Electron. Syst.*, vol. 47, no. 1, pp. 596–610, Jan. 2011.
[20] S. Park, C.-W. Tan, and J. Park, "A scheme for improving the performance of a gyroscope-free inertial measurement unit," *Sens. Actuators A, Phys.*, vol. 121, no. 2, pp. 410–420, Jun. 2005. [Online]. Available: https://www.sciencedirect.com/science/article/pii/S0924424705001366
[21] C.-W. Tan and S. Park, "Design and error analysis of accelerometer-based inertial navigation systems," Inst. Transp. Stud., UC Berkeley, Berkeley, CA, USA, Tech. Rep. UCB-ITS-PRR-2002-21, 2002.
[22] C.-W. Tan, K. Mostov, and P. Varaiya, "Feasibility of a gyroscope-free inertial navigation system for tracking rigid body motion," Inst. Transp. Stud., UC Berkeley, Berkeley, CA, USA, Tech. Rep. UCB-ITS-PRR-2000-9, 2000.
[23] C.-W. Tan, S. Park, K. Mostov, and P. Varaiya, "Design of gyroscope-free navigation systems," in *Proc. IEEE Intell. Transp. Syst.*, Aug. 2001, pp. 286–291.
[24] S. Park and C.-W. Tan, "GPS-aided gyroscope-free inertial navigation systems," Inst. Transp. Stud., UC Berkeley, Berkeley, CA, USA, Tech. Rep. UCB-ITS-PRR-2002-22, 2002.
[25] E. Akeila, Z. Salcic, and A. Swain, "Implementation, calibration and testing of GFINS models based on six-accelerometer cube," in *Proc. IEEE Region 10 Conf.*, Nov. 2008, pp. 1–6.
[26] S. Skogestad and I. Postlethwaite, *Multivariable Feedback Control: Analysis and Design*. Hoboken, NJ, USA: Wiley, 2005.
[27] G. Strang, *Linear Algebra and Its Applications*. Salt Lake City, UT, USAL Brooks Cole/Cengage Learning, 2007.
[28] T. W. Anderson, *An Introduction to Multivariate Statistical Analysis*. Hoboken, NJ, USA: Wiley, 2003.
[29] *BNO055—Intelligent 9-Axis Absolute Orientation Sensor*, BST-BNO055-DS000-14, Bosch Sensortec, Kusterdingen, Germany, 2016.

**Konstantinos Papafotis** (Member, IEEE) received the Diploma degree in electrical and computer engineering from the National Technical University of Athens, Athens, Greece, in 2015, and the Ph.D. degree from the National Technical University of Athens, under the supervision of Prof. Paul P. Sotiriadis. His Ph.D. thesis is about calibration methods and applications of inertial and magnetic field sensors in the field of navigation.

He is the author of several conference papers and journal articles. His main research interests include inertial navigation, embedded systems, and wireless sensors' systems.

Dr. Papafotis received the Best Paper Award at the IEEE International Conference on Modern Circuits and Systems Technologies in 2019. He is a regular reviewer for many IEEE publications.

**Dimitris Nikitas** received the Diploma degree in electrical and computer engineering from the National Technical University of Athens, Athens, Greece, in 2021, under the supervision of Prof. Paul P. Sotiriadis. He is currently pursuing the M.Sc. degree in systems and control with the Eidhoven University of Technology, Eindhoven, The Netherlands.

He is the author of several conference papers and journal articles. His main research interests include control theory, robotics, and inertial navigation.

Mr. Nikitas has reviewed the IEEE SENSORS JOURNAL. He is a regular reviewer for many IEEE publications.

**Paul P. Sotiriadis** (Senior Member, IEEE) received the Diploma degree in electrical and computer engineering from the Electrical and Computer Engineering Department, National Technical University of Athens, Athens, Greece, in 1994, the M.S. degree in electrical engineering from Stanford University, Stanford, CA, USA, in 1996, and the Ph.D. degree in electrical engineering and computer science from the Massachusetts Institute of Technology, Cambridge, MA, USA, in 2002.

He is a Faculty Member with the Electrical and Computer Engineering Department, National Technical University of Athens, where he is the Director of the Electronics Laboratory, and a member of the Governing Board of the Hellenic Space Center, National Space Center of Greece. In 2002, he joined Johns Hopkins University, Baltimore, MD, USA, as an Assistant Professor of Electrical and Computer Engineering. In 2012, he joined the faculty of the Electrical and Computer Engineering Department, National Technical University of Athens. He has led several projects in these fields funded by U.S. organizations and has collaborations with industry and national laboratories. He has authored and coauthored more than 150 research publications, most of them in IEEE journals and conferences, holds one patent, and has contributed chapters to technical books. His research interests include design, optimization, and mathematical modeling of analog and mixed-signal circuits, RF and microwave circuits, advanced frequency synthesis, biomedical instrumentation, and interconnect networks in deep-submicrometer technologies.

Dr. Sotiriadis has been a member of technical committees at many conferences. He has received several awards, including the 2012 Guillemin-Cauer Award from the IEEE Circuits and Systems Society, the Best Paper Award at the IEEE International Symposium on Circuits and Systems in 2007, the Best Paper Award at the IEEE International Frequency Control Symposium 2012, and the Best Paper Award at the IEEE International Conference on Modern Circuits and Systems Technologies in 2019. He is an Associate Editor of the IEEE SENSORS JOURNAL. He has served as an Associate Editor for the IEEE TRANSACTIONS ON CIRCUITS AND SYSTEMS I: REGULAR PAPERS from 2016 to 2020 and the IEEE TRANSACTIONS ON CIRCUITS AND SYSTEMS II: EXPRESS BRIEFS from 2005 to 2010. He regularly reviews for many IEEE TRANSACTIONS and conferences and serves on proposal review panels.